

Single-Layer Learnable Activation for Implicit Neural Representation (SL²A-INR)

Moein Heidari^{1*}, Reza Rezaeian^{2*}, Reza Azad³, Dorit Merhof⁴, Hamid Soltanian-Zadeh^{2,5†}, Ilker Hacihaliloglu^{6‡}

¹School of Biomedical Engineering, University of British Columbia, Vancouver, BC, Canada

²School of Electrical and Computer Engineering, College of Engineering, The University of Tehran, Iran

³Faculty of Electrical Engineering and Information Technology, RWTH Aachen University Aachen, Germany

⁴Faculty of Informatics and Data Science, University of Regensburg Regensburg, Germany

⁵Medical Image Analysis Laboratory, Department of Radiology, Henry Ford Health System, Detroit, Michigan, USA

⁶Department of Radiology, Department of Medicine, University of British Columbia, Vancouver, BC, Canada

{moein.heidari, ilker.hacihaliloglu}@ubc.ca, {r.rezaeian, hszadeh}@ut.ac.ir,

reza.azad@rwth-aachen.de, dorit.merhof@ur.de

Abstract

Implicit Neural Representation (INR), leveraging a neural network to transform coordinate input into corresponding attributes, has recently driven significant advances in several vision-related domains. However, the performance of INR is heavily influenced by the choice of the nonlinear activation function used in its multilayer perceptron (MLP) architecture. Multiple nonlinearities have been investigated; yet, current INRs face limitations in capturing high-frequency components, diverse signal types, and handling inverse problems. We have identified that these problems can be greatly alleviated by introducing a paradigm shift in INRs. We find that an architecture with learnable activations in initial layers can represent fine details in the underlying signals. Specifically, we propose SL²A-INR, a hybrid network for INR with a single-layer learnable activation function, prompting the effectiveness of traditional ReLU-based MLPs. Our method performs superior across diverse tasks, including image representation, 3D shape reconstructions, inpainting, single image super-resolution, CT reconstruction, and novel view synthesis. Through comprehensive experiments, SL²A-INR sets new benchmarks in accuracy, quality, and convergence rates for INR.

1 Introduction

Implicit neural representations (INRs), which model continuous functions over discrete data points, have recently garnered significant attention for their ability to effectively represent 2D images, 3D shapes, neural radiance fields, and other complex structures (Mildenhall et al. 2021; Sitzmann et al. 2020; Park et al. 2019; Shi, Zhou, and Gu 2024). Unlike traditional discrete grid-based methods, INRs focus on training neural networks, particularly Multilayer Perceptrons (MLPs), that utilize continuous element-wise nonlinear activation functions to map continuous input coordinates to their respective output values, thereby delivering a continuous signal representation (Sitzmann et al. 2020). Due to

their flexible, compact and efficient design, INRs have garnered immense interest in solving tasks dealing with complex and high-dimensional data. They have demonstrated versatility across a wide range of applications, including computer graphics (Mildenhall et al. 2021; Müller et al. 2022; Chen et al. 2024), computer vision (Maiya et al. 2023; Zhu et al. 2024), inverse problems (Sun et al. 2021), and signal representations (Xu et al. 2022; Sitzmann et al. 2020), enabling adaptive compression schemes tailored to the content's complexity (Heidari et al. 2024b,a). In contrast to Convolutional Neural Networks (CNNs), INRs are not constrained by locality biases, thus exhibit exceptional generalization abilities, feature a concise formulation, and display enhanced flexibility. However, their potential is constrained by various obstacles that limit the application of INRs. Conventional neural networks like ReLU-based MLPs struggle to capture high-frequency details accurately in signals, such as intricate textures in images or complex shapes in 3D reconstruction, due to their inherent bias towards learning simpler, lower-frequency patterns, known as spectral or low-frequency bias (Rahaman et al. 2019; Xu 2018). The trailblazing efforts in mitigating this issue can be roughly grouped into several main categories. One approach involves increasing the complexity of the input data manifold and explicitly extracting high-frequency features, such as through positional encoding (Tancik et al. 2020; Müller et al. 2022). An alternative major category of methods utilizes complicated activation functions to achieve more precise approximations (Sitzmann et al. 2020; Fathony et al. 2020; Saragadam et al. 2023). Despite yielding promising results, these approaches still exhibit some degree of spectral bias (Yüce et al. 2022), primarily learning faster lower-frequency components of the input. This indicates that there is still room for improvement in addressing spectral bias more comprehensively (Cai et al. 2024). Moreover, periodic activation functions are particularly vulnerable to initialization methods, experiencing notable performance declines when not strictly following initialization protocols (Ramasininghe and Lucey 2022). Therefore, these approaches have difficulty representing fine details in complex shapes, limiting their flexibility across signal types and inverse problems. To overcome these challenges, we propose a novel approach that

*Equal contribution.

†Corresponding author.

‡Corresponding author.

significantly boosts the hierarchical representation capabilities of INRs. Our method achieves superior performance in high-fidelity reconstructions across a wide array of tasks, including images and intricate 3D structures. Additionally, it addresses complex problems such as Neural Radiance Fields (NeRF) and inverse problems, including super-resolution, inpainting, and computed tomography (CT) reconstruction. Specifically, the common behavior of MLP networks in the early layers is for neurons to select low-frequency features in the data, which causes higher frequencies to be learned later in the optimization process (Rahaman et al. 2019). Inspired by this, we hypothesize that an accurate polynomial approximation of activation functions in the initial layer of INRs will be sufficient for capturing the high-frequency, fine-grained details and that the spectral spread is influenced by the magnitude of higher-order polynomial coefficients (Mehmeti-Göpel, Hartmann, and Wand 2020). To achieve this, we utilize the stable and non-oscillatory Chebyshev approximation method and propose a ***Learnable Activation (LA)*** Block which allows for the capture of finer details and higher frequency components in the function being approximated, while being able to perform spectral-bias adjustment using the Chebyshev coefficients adaptively. Furthermore, we modulate the high-frequency signal passing through the network by adding skip connections to the subsequent ReLU-based MLPs in our ***Fusion Block***. This arrangement empowers the network to integrate elements to capture a broad spectrum of frequencies in the input signal, ultimately addressing the challenge of spectral bias. Our comprehensive experiments across diverse applications clearly showcase the superiority of our approach in robustness, accuracy, quality, and convergence rate.

Contributions In summary, this paper offers the following contributions:

- We introduce a novel implicit neural representation with learnable activation functions, which allows for capturing finer details and higher frequencies.
- We conduct extensive experiments across various INR tasks, demonstrating that our approach enhances SOTA architectures by capturing more high-frequency details.
- We provide a comprehensive ablation study that equips insight into the specifics and design choices of our method.

2 Related Works

Implicit Neural Representation Recent studies have demonstrated significant success in utilizing neural networks for representing various types of signals. These representations are applied across a range of applications, including images (Ramasinghe and Lucey 2022; Saragadam et al. 2023; Sitzmann et al. 2020), occupancy volumes (Ortiz et al. 2022), view synthesis (Mildenhall et al. 2021; Bian et al. 2023; Gao et al. 2022), and audio/video signals (Su, Chen, and Shlizerman 2022; Chen et al. 2022). However, the widely-used ReLU activation function has limitations in learning low-frequency information, which can affect the performance of standard MLPs (Tancik et al. 2020). In this

context, the ReLU activation function often fails to accurately represent the signal, resulting in the loss of important high-frequency components and leading to a suboptimal overall representation. To address this issue, several solutions have been proposed in the literature. One approach involves encoding the input data with sinusoids (Tancik et al. 2020), which maps the input coordinates to a higher dimensional space. The output of this positional encoding is then used as input to the MLP. Another line of research focuses on modifying the activation functions of the MLP. For instance, using periodic activations as in SIREN (Sitzmann et al. 2020), Gaussian activations (Ramasinghe and Lucey 2022), or wavelet-based activations (Saragadam et al. 2023) can help capture high-frequency details more effectively. However, these methods also come with their own challenges. For example, the representational capacity of SIREN can be highly dependent on the choice of hyperparameters for sinusoidal functions, such as frequency, and can be sensitive to initialization, necessitating careful design choices to avoid random variations (Vonderfecht and Liu 2024).

Learnable Activation Functions As previously noted, the methods for mitigating spectral bias in INRs have introduced new challenges. In particular, networks utilizing custom activation functions, such as periodic activations, are highly sensitive to initialization schemes and hyperparameter choices. Specifically, the inherent periodicity of sine functions can cause oscillations and slow down convergence, creating challenges during the training process (Liu et al. 2024b). Additionally, despite advancements, some degree of spectral bias remains present in these approaches. Consequently, it is critical to develop an adaptive function to handle nonlinearity and complex frequency distribution effectively. Instead of relying solely on custom-designed activation functions, which may have their own limitations, we propose using learnable activation functions that adapt based on the data itself as part of our network. A learnable activation function is a type of activation function in neural networks that is not fixed but is optimized during training. Unlike traditional activation functions, which are predetermined and static, learnable activation functions have parameters that are adjusted through backpropagation (Goyal, Goyal, and Lall 2019; Bingham and Miikkulainen 2022). These functions can be represented by various forms, such as polynomials, splines, or sigmoid linear units (Goyal, Goyal, and Lall 2019; Fakhouri, Fakhouri, and Speleers 2022; Ramachandran, Zoph, and Le 2017), and are designed to adapt dynamically to the data and learning process, potentially enhancing the network’s ability to capture complex patterns and improve performance. Specifically, the recent Kolmogorov-Arnold Network (KAN) (Liu et al. 2024a) utilizes B-splines for their activation functions. Capitalizing on this line of research, we transform the input coordinates into a high-dimensional space by projecting them onto multiple adaptive Chebyshev polynomial (SS et al. 2024) functions of a fixed degree, departing from the fixed activation functions or positional encodings. These polynomials act as learnable activations, allowing the network to adaptively capture a wide spectrum of frequency information by leveraging the spectral properties of Chebyshev polynomials to efficiently

represent both low and high-frequency components of the input signal. Besides, we incorporate a feature interaction mechanism where the Learnable Activation (LA) Block’s output serves as a dynamic modulator for subsequent layers, enhancing the model’s ability to capture and propagate high-frequency features throughout the network.

3 Method

Preliminary

Instead of relying on traditional discrete data structures like pixels or voxels, INRs encode information within the weights and structure of a neural network. Mathematically, this can be expressed as a neural network f_θ , where θ represents the parameters of the network. The input \mathbf{x} typically denotes coordinates (e.g., spatial coordinates in an image), and the output \mathbf{y} represents the corresponding signal values (e.g., intensity values in an image). Formally, this relationship is defined as:

$$\mathbf{y} = f_\theta(\mathbf{x}) \quad (1)$$

this neural network is trained using the mean squared error (MSE) loss. The MSE loss function is defined as:

$$\mathcal{L}(\theta) = \frac{1}{N} \sum_{i=1}^N (f_\theta(\mathbf{x}_i) - \mathbf{y}_i)^2 \quad (2)$$

where \mathbf{x}_i are the input coordinates, \mathbf{y}_i are the true signal values, and N is the number of training samples.

SL²A-INR

Given the challenges of specific activation function designs, a key question arises: Can traditional ReLU-based MLPs be modified to enhance learning and mitigate spectral bias? We propose a solution by altering only the input layer to incorporate learnable activation functions while redesigning subsequent layers to leverage the learned features. As depicted in Fig. 1, our architecture consists of two blocks: a learnable activation function in the first block for feature extraction, followed by a ReLU-based MLP that exploits these features. Detailed structural insights are provided in the subsequent subsections.

Learnable Activation (LA) Block Drawing inspiration from the Kolmogorov-Arnold representation theorem (Kolmogorov 1961) and a recent study (Liu et al. 2024a) employing learnable activations on edges—instead of nodes—as in vanilla MLPs, we introduce our initial block where we parameterize this block with high-degree polynomials to effectively learn these activations. Assuming the input dimension n and the output dimension of the block is m , following (Liu et al. 2024a), we define the first block as:

$$\Psi(\mathbf{X}_{\text{in}}) = \begin{pmatrix} \psi_{1,1}(\cdot) & \psi_{1,2}(\cdot) & \cdots & \psi_{1,n}(\cdot) \\ \psi_{2,1}(\cdot) & \psi_{2,2}(\cdot) & \cdots & \psi_{2,n}(\cdot) \\ \vdots & \vdots & \ddots & \vdots \\ \psi_{m,1}(\cdot) & \psi_{m,2}(\cdot) & \cdots & \psi_{m,n}(\cdot) \end{pmatrix} \begin{pmatrix} x_1 \\ x_2 \\ \vdots \\ x_n \end{pmatrix} \quad (3)$$

Where each $\psi_{i,j}$ denotes a learnable one-dimensional function applied independently to the corresponding feature of

the input. These learnable functions can be parameterized in various ways, such as using B-splines (Liu et al. 2024a) or polynomials (SS et al. 2024). We parametrize ψ as a linear combination of Chebyshev polynomials with degrees ranging from 1 to D . The equation can be written as:

$$\psi(x) = \sum_{d=1}^D a_d T_d(x) \quad (4)$$

where T_d is the Chebyshev polynomial of degree d and a_d is the learnable coefficient. We argue that a single layer of these high-degree polynomial-parameterized activations is enough to achieve a strong representation in the first block. This representation can then be effectively used in the following blocks to build a neural network that trains efficiently and avoids spectral bias. As part of the implementation detail, input coordinates \mathbf{x} in the first block are initially normalized to the $[-1, 1]$ range using the hyperbolic tangent function (\tanh), aligning with the domain of Chebyshev polynomials. The Learnable Activation (LA) block then processes these normalized inputs, followed by layer normalization.

Fusion Block We define the Fusion Block as a stack of several hidden layers, each consisting of a linear map followed by a simple non-linear activation function like ReLU. Since these layers act like a low-pass filter (Wu, Jin, and Yi 2023), we modulate the output of the previous layer with the output of the initial Learnable Activation (LA) Block. Mathematically, each layer in the Fusion Block can be defined as:

$$\mathbf{y}_l = \sigma(\mathbf{W}_l(\mathbf{y}_{l-1} \odot \Psi(\mathbf{X}_{\text{in}})) + \mathbf{b}_l) \quad (5)$$

for $l = 2, 3, \dots, L-1$, where \mathbf{y}_l is the output of the l -th layer, \mathbf{W}_l and \mathbf{b}_l are the weights and biases of the l -th layer, σ denotes the ReLU activation function, $\Psi(\mathbf{X}_{\text{in}})$ is the output of the Learnable Activation Block, and \odot represents the Hadamard (element-wise) product. This modulation improves the performance of the model by dynamically adjusting the influence of each hidden layer based on the initial Learnable Activation Block. This dynamic adjustment helps in capturing more intricate patterns and reduces the spectral bias, ultimately leading to enhanced representation capabilities and better overall performance. A simpler architecture could involve using an MLP as the second block to receive the output from the first block. However, as demonstrated in our ablation study, this approach significantly reduces performance, highlighting the importance of our design.

4 Experimental Results

To evaluate the effectiveness of our proposed method, we conducted several experiments in signal representation tasks and inverse problems, such as 2D image representation, 3D shape reconstruction, CT reconstruction, single-image super-resolution, and image inpainting. Our experiments were conducted using PyTorch on an Nvidia RTX 4070 GPU equipped with 12GB of memory. Unless specified otherwise, we employed a 5-layer neural network with 256 units in hidden layers for all experiments. For the hyperparameters of

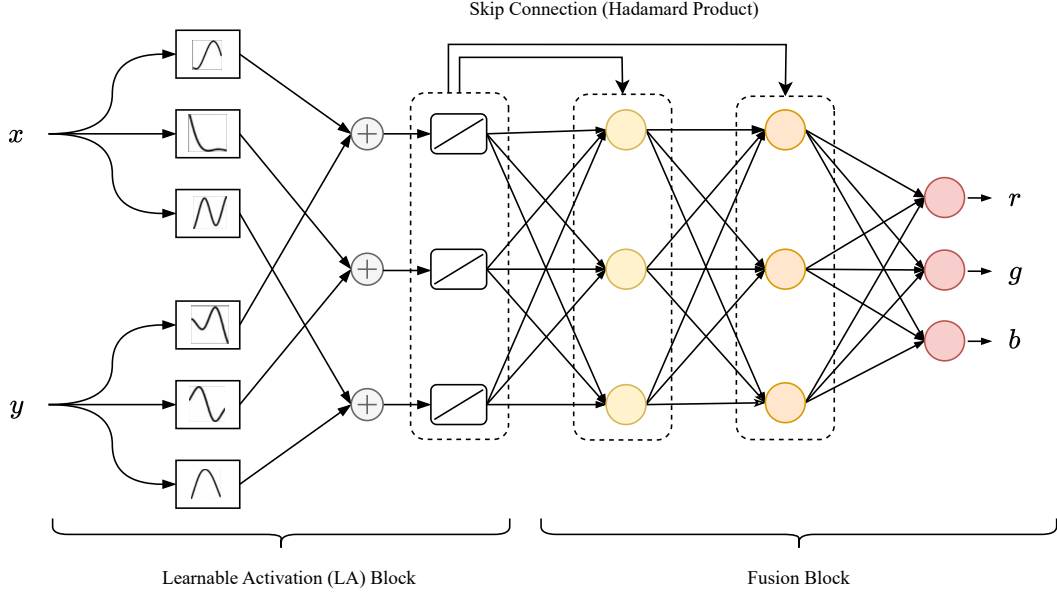


Figure 1: Illustration of the SL^2A -INR pipeline.

our baseline methods, we followed the configurations specified in Incode (Kazerouni et al. 2024), except for the learning rate and batch size, which were optimized through a grid search. Notably, we used all configurations from (Saragadam et al. 2023) for occupancy representation. We explored all possible combinations of learning rates (1e-4, 1e-3, 1e-2) and batch sizes (32×32, 64×64, 128×128, 256×256). For each combination, we ran each model on five different images, averaging the results to select the best configuration of learning rate and batch size. For our model, we used the same configurations of learning rate and batch size as the best-performing ReLU+P.E. (Tancik et al. 2020) model.

Signal Representations

Image Representation We first applied our method to the task of 2D image fitting using INR. In our model, the first layer employs high-degree Chebyshev polynomials (degree=512), while the subsequent layers use simple ReLU activation functions. The loss function used is the MSE between the model’s output and the actual pixel values in the images.

Data For our image representation experiments, we used the DIV2K dataset (Timofte et al. 2017), which we down-scaled by a factor of 1/4. The resulting image had dimensions $510 \times 342 \times 3$ and exhibited varying levels of detail across its regions.

Results We compared our method with six baselines: WIRE (Saragadam et al. 2023), SIREN (Sitzmann et al. 2020), INCODE (Kazerouni et al. 2024), MFN (Fathony et al. 2020), ReLU+P.E. (Tancik et al. 2020), and Gauss (Ramasinghe and Lucey 2022). We trained each model for 500 epochs and reported the best results. All models have the same architec-

ture with three hidden layers and 256 neurons in each hidden layer, except for WIRE, for which we followed their paper and used an MLP with two hidden layers of 300 hidden features. As shown in Fig. 2, our method achieves the best qualitative and quantitative results, with a PSNR approximately 11 dB higher than the best baseline, INCODE (Kazerouni et al. 2024). Our model not only reconstructs fine details but also preserves the uniformity of black regions, unlike other methods that introduce noise. The green boxes in the figure highlight areas where our model excels in maintaining detail and texture.

Occupancy Volume Representation For this task, we use the WIRE configuration (Saragadam et al. 2023), where our network translates 3D coordinates ($M = 3$) into signed distance function (SDF) values ($N = 1$).

Data We utilize the Thai statue dataset obtained from the Stanford 3D Scanning Repository, and similar to (Saragadam et al. 2023), we performed sampling on a $512 \times 512 \times 512$ grid, where each voxel inside the volume was given a value of 1 and those outside were given a value of 0. Different approaches were assessed using the intersection over union (IOU) metric for these occupancy volumes.

Results Fig. 3 provides comparisons between the proposed method and four baselines showing superior reconstruction quality. Specifically, both low-frequency smooth regions (the torsos), and the high-frequency rough parts (feet of the statue) are well represented by SL^2A -INR, providing consistent performance as opposed to other methods. This balanced representation is attributed to our method’s synergistic design, which combines the fusion blocks for capturing low-frequency components with a learnable activation block specialized in high-frequency learning, allowing for a

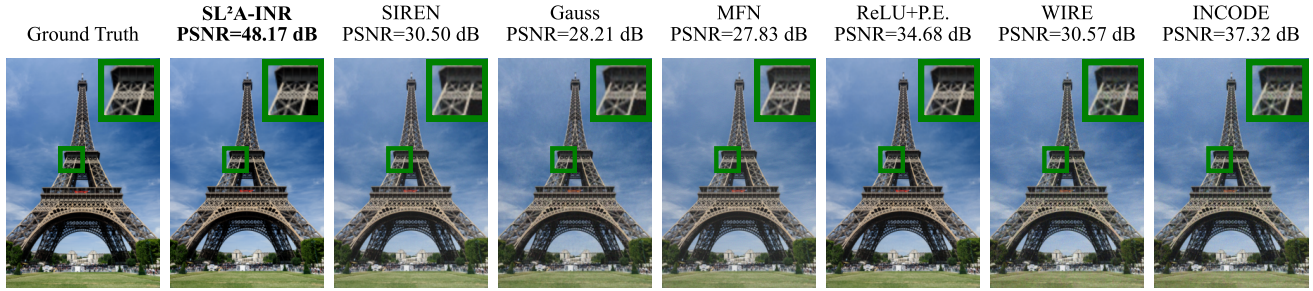


Figure 2: Comparison of image representation of $\text{SL}^2\text{A-INR}$ with other methods.

comprehensive spectral representation with the highest IOU values.

Inverse Problems

Inverse problems are inherently challenged by robustness issues, particularly when dealing with noisy and undersampled data. This complexity arises because the inverse problem necessitates precise fitting of the supervised values and accurate interpolation between these values. To validate the effectiveness of $\text{SL}^2\text{A-INR}$, we assess it on three such tasks.

Super Resolution We maintain our architecture for the image representation, adjusting only the degree of the Chebyshev coefficient to 200.

Data We evaluate our method on an image from DIV2K dataset (Timofte et al. 2017). The original image, with dimensions $1356 \times 2040 \times 3$, is downsampled by a 1/4 factor.

Results Fig. 4 illustrates the 4 \times super-resolution results of a parrot image using various methods. The findings indicate that $\text{SL}^2\text{A-INR}$ consistently achieves higher PSNR and SSIM (Hore and Ziou 2010) values, surpassing other techniques. Additionally, the visual results highlight $\text{SL}^2\text{A-INR}$ ’s capability to preserve sharper details, whereas other methods tend to produce blurrier images. Specifically, our method delivers the sharpest outcome, capturing clear and crisp details on the parrot’s feathers and beak.

Computed Tomography Reconstruction Our network is similar to that used in the image representation task, except that the Chebyshev degree was adjusted to 128.

Data We evaluated our method on the CT reconstruction task using an image from the lung segmentation dataset introduced in the Lung Nodule Analysis (LUNA) competition on Kaggle (Azad et al. 2019), which has a resolution of 256×256 and is emulated with 100 CT measurements.

Results Projection data in CT imaging are measured to enable lower radiation doses for patients. Reducing the number of measurements required for high-quality image reconstruction is often desirable, but the information loss from sparse sampling makes this reconstruction process challenging and ill-posed in both industrial and medical settings. $\text{SL}^2\text{A-INR}$ addresses these challenges by representing the high-frequency variations in the measurement field while avoiding strong artifacts in the generated measurements. Specifically, as it can be observed from Fig. 5, our method

achieves the highest PSNR among all tested methods, significantly enhancing reconstruction quality by effectively capturing finer details. INCODE and WIRE, despite having similar quantitative performance to ours, lead to excessively smooth results, only displaying blurry patterns. The result of ReLU+P.E and SIREN are noisy, failing to exhibit the precise details, while MFN shows artifacts similar to Gauss. In contrast, $\text{SL}^2\text{A-INR}$ highlights strength in tackling the difficulties of noisy and undersampled inverse problems. By effectively harmonizing image fidelity and noise mitigation, $\text{SL}^2\text{A-INR}$ emerges as a compelling approach for tackling the intricate domain of image reconstruction where constraints are limited, as demonstrated across three diverse tasks in this section. We show the effectiveness of our approach in inpainting and neural radiance fields (NeRF) tasks through comparative analysis, with additional results in the supplementary material.

5 Analysis

In this section, we delve into the impact of various design choices on the model’s overall performance. To this end, we conducted a thorough ablation study, examining the effects of model size, the influence of our method on frequency analysis, the role of the fusion block, and a comparative analysis of the convergence rates of different methods presented in the supplementary materials.

Spectral Bias

In (Rahaman et al. 2019), the authors show that MLP-based networks have a frequency-dependent learning speed and they find empirical evidence of a spectral bias, i.e., lower frequencies are learned first. To explore the spectral bias of our network, following the experimental setting in (Shi, Zhou, and Gu 2024), we used a 1D rounded periodic function with four different major frequencies in that spectrum as Equation 6. The function $f(x)$ has 300 discrete values uniformly sampled in the interval $[-1, 1]$. We used an MLP with three hidden layers, each with 128 neurons, and the degree of polynomials in our method is 64.

$$f(x) = 2R \left(\frac{\sin(3\pi x) + \sin(5\pi x) + \sin(7\pi x) + \sin(9\pi x)}{2} \right) \quad (6)$$

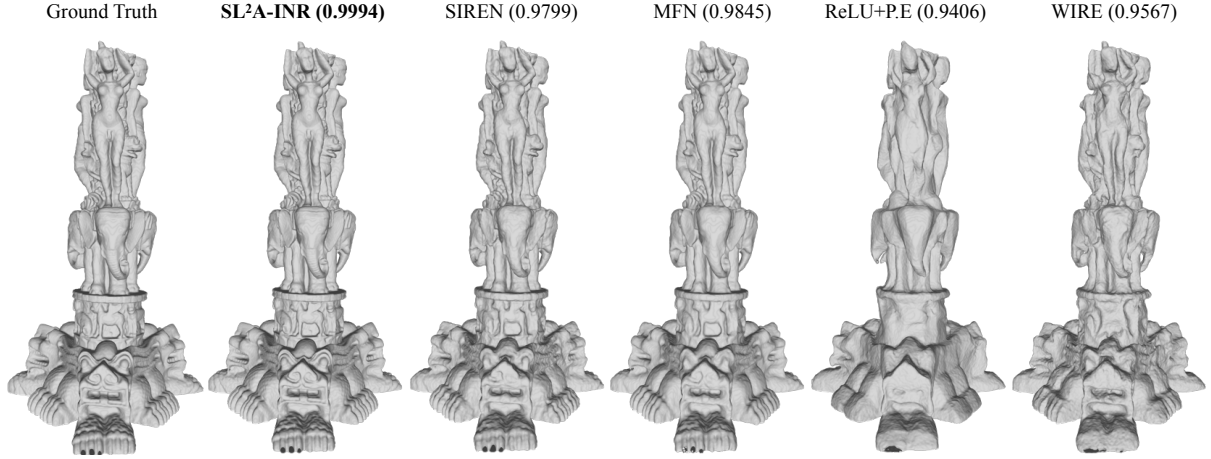


Figure 3: Results for occupancy with different methods. The numbers in parentheses represent the IoU metric.

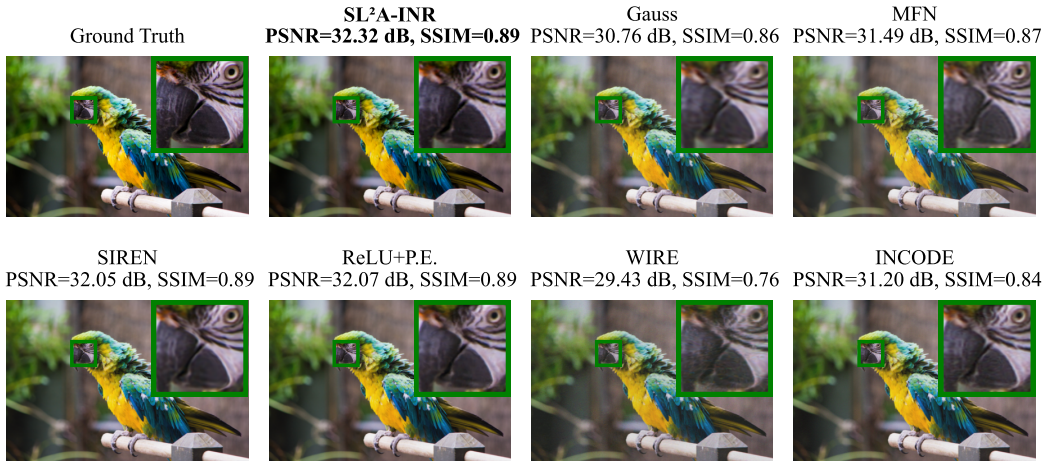


Figure 4: Results for a 4x single image super resolution with different methods.

Here, R denotes the rounding function, which makes the data more challenging to train by introducing discontinuities. To investigate the effectiveness of our method, we trained both our method and SIREN on this data and compared the frequency-dependent learning speed of both methods. As shown in Fig. 6, SIREN exhibits spectral bias, learning low-frequency information faster while struggling to capture high-frequency components. In contrast, our method balances the learning of both low and high frequencies, showing no spectral bias.

Effect of Model Size

As shown in Fig. 2, compared to other methods, our model demonstrates a high capacity for fitting 2D images. This is achieved by introducing high-degree learnable polynomials in the first layer, which also increases the size of the neural network. To determine if these results are due to the model size, we introduce two variants of the model. In the first variant, we replace all linear layers from the second layer onward with low-rank linear layers (rank=32) and use poly-

nomials of degree 256 in the first layer to reduce the number of parameters, making it comparable to other baselines. The second variant is identical to the base model but has 128 neurons in each hidden layer (half the number of neurons in the hidden layers of other baselines), and the polynomials in the first layer have a degree of 500, which reduces the model size to be smaller than that of other baselines. The quantitative results are presented in Table 1 and are further demonstrated with qualitative results in the supplementary materials. Our variants, even with the smallest size, achieve superior results, demonstrating the effectiveness of our proposed architectural bias.

Importance of Fusion Block

To demonstrate the effectiveness of utilizing skip connections for filtering high-frequency details in subsequent layers, we conducted image fitting experiments by disconnecting the skip connections, reducing the fusion block to a simple MLP. As shown in Table 2, disconnecting these connections in the simple model results in reduced PSNR for three

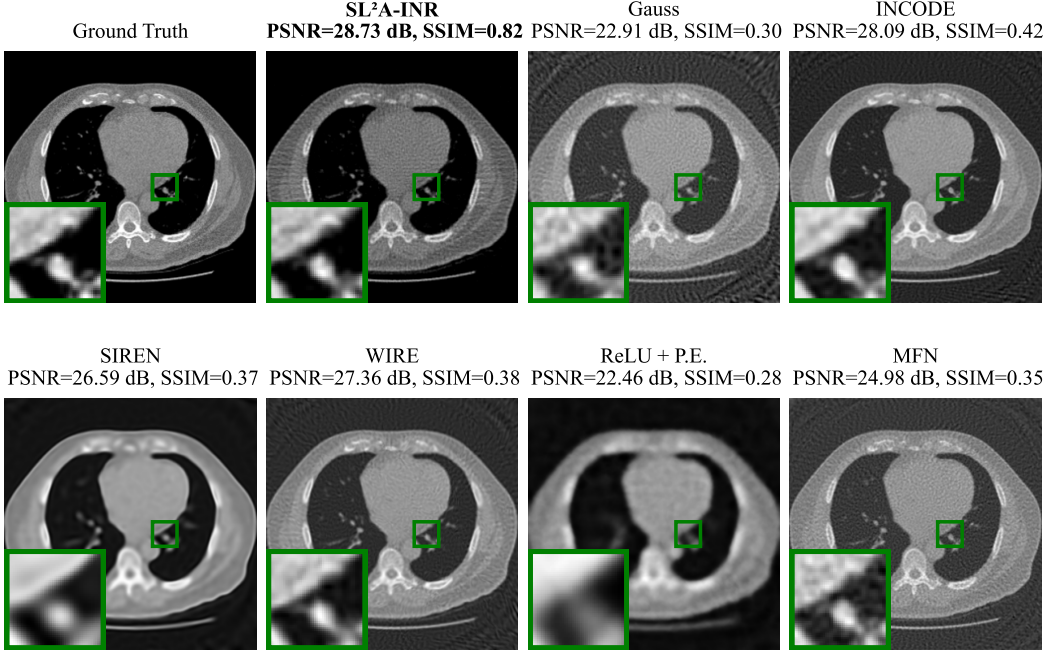


Figure 5: Results of CT reconstruction with 100 angles with different methods.

	#Params (M)↓	Plant		Castle	
		PSNR↑	SSIM↑	PSNR↑	SSIM↑
SIREN (Müller et al. 2022)	0.198	38.21	0.9588	30.54	0.8723
Gauss (Ramasinghe and Lucey 2022)	0.198	41.51	0.9724	28.29	0.8348
MFN (Fathony et al. 2020)	0.204	39.64	0.9710	31.24	0.8905
ReLU+PE (Tancik et al. 2020)	0.204	45.85	0.9814	34.05	0.9277
INCODE (Kazerouni et al. 2024)	0.198	38.42	0.9814	35.86	0.9277
SL ² A-INR-width256	0.461	54.58	0.9922	46.84	0.9920
SL ² A-INR-width256-low-rank	0.190	48.02	0.9844	37.93	0.9611
SL ² A-INR-width128	0.181	46.72	0.9826	36.37	0.9399

Table 1: **2D Image Representation (Blue indicates the best result, and red displays the second-best.)** – Our method achieves superior performance across its various variants. Even the smaller variants, despite their reduced size compared to other methods, perform well in terms of Peak Signal-to-Noise Ratio (PSNR) and Structural Similarity Index Metric (SSIM).

	Plant	Castle	Eiffel
	PSNR↑	PSNR↑	PSNR↑
Full Model	54.58	46.84	48.17
Simple Model	51.43	45.35	46.69

Table 2: Comparing different model variants based on skip connection.

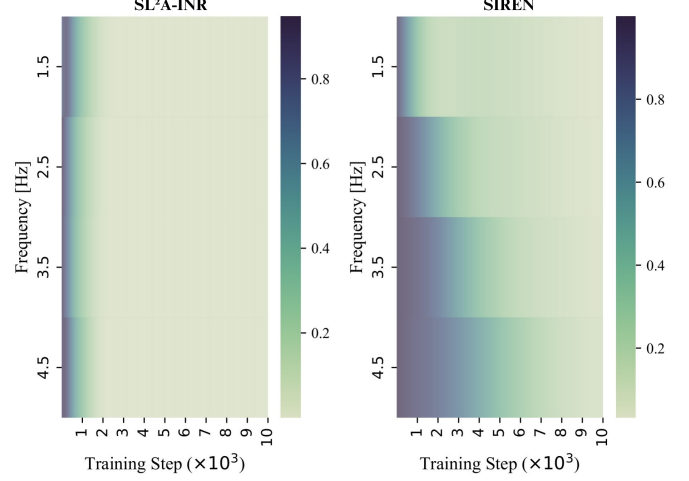


Figure 6: Comparison of frequency-dependent learning speed between SIREN and our method. The x-axis represents the training step, the y-axis represents the frequency, and the colormap indicates the relative approximation error.

different images, yielding worse outcomes compared to the proposed base model.

6 Conclusion

We introduced and validated the SL²A-INR, a novel approach to INRs that enhances their representation capability. We identified that current INRs have a limited frequency set, and existing solutions lack generalization and require

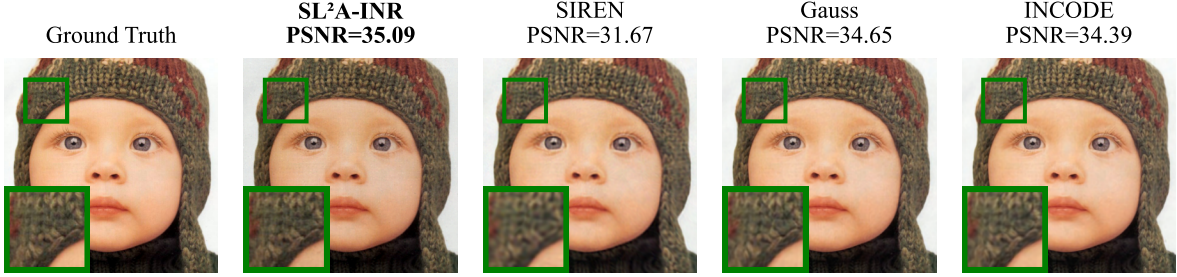


Figure 7: Results of image inpainting experiment for different methods.



Figure 8: **Neural Radiance Fields:** The figure shown above displays images produced by a neural radiance field through various methods. SL²A-INR consistently delivers superior visual reconstruction quality, demonstrating its strong capability in feature representation.

parameter tuning. Our SL²A-INR solves this using a learnable activation layer, which concomitantly captures multiple frequencies and leverages the learned features from this layer in subsequent ReLU-based MLP layers, enabling concomitant capture of different frequencies across the definition domain. We have shown that SL²A-INR outperforms other INRs across a range of tasks, including image fitting, 3D shape representation, and inverse problems.

7 Supplementary Material

This supplementary material contains the following additional information. We further substantiate the optimality of our approach through its application to two additional tasks: inpainting and neural radiance fields. These tasks not only reinforce the robustness of our method but also demonstrate its adaptability across diverse domains. Additionally, we delve into the implications of model size and provide a comprehensive analysis of convergence rates across different tasks, underscoring the versatility and efficiency of our solution.

A Image Inpainting

For this task, our network architecture closely resembles the one employed for the image representation.

Data: We employ an image of a baby from the Set5 dataset (Zeyde, Elad, and Protter 2012) with a resolution of $512 \times 512 \times 3$. The sampling mask is created randomly, ensuring that, on average, 70% of the pixels are selected to better represent real-world inpainting problems.

Results: As presented in Fig. 7, SL²A-INR excels in capturing intricate features, especially edges, standing out from other methods that often produce blurry results where finer details become lost. Although it edges out Gauss (Ramasinhe and Lucey 2022) with a modest improvement $+0.44dB$, the visual results show that Gauss, similar to SIREN (Sitzmann et al. 2020) and INCODE (Kazerouni et al. 2024), struggles to capture the full range of detail, leaving things blurry.

B Neural radiance fields

Neural Radiance Fields (NeRFs) (Mildenhall et al. 2021) is a technique for synthesizing novel views of complex 3D scenes by representing them as continuous volumetric func-

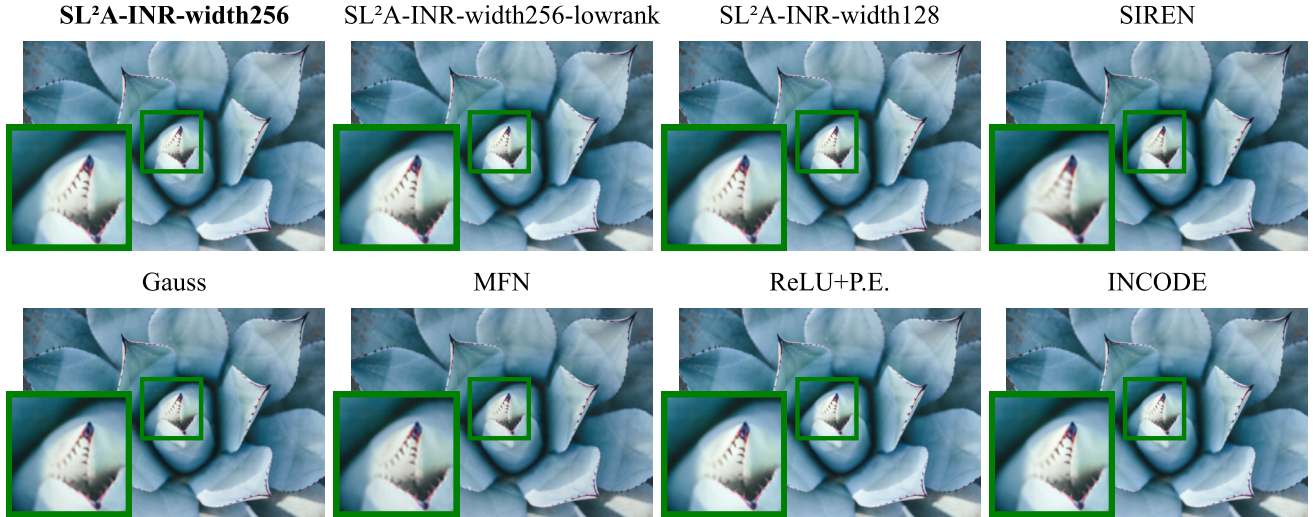


Figure 9: Comparison of image representation of $\text{SL}^2\text{A-INR}$ with other methods.

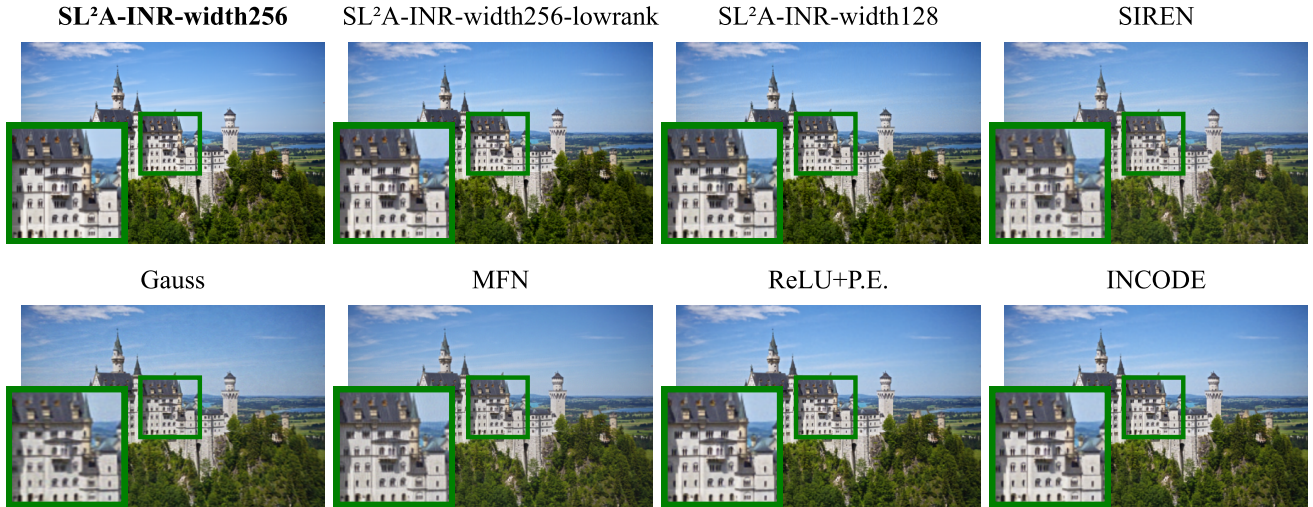


Figure 10: Comparison of image representation of $\text{SL}^2\text{A-INR}$ with other methods.

tions optimized using 2D images and camera poses. The architecture utilizes an MLP to implicitly encode the scene, taking 5D coordinates—3D spatial location and 2D viewing direction—as inputs, and outputting the corresponding RGB color and volume density. We follow the setup outlined in (Kazerouni et al. 2024) for training to facilitate the comparison of different baselines. Specifically, we employed a Lego dataset containing 100 images for training, where each image was downsampled by half to a resolution of 400×400 pixels to train the NeRF model. The model’s performance was then assessed using an additional set of 200 images. Our network architecture is identical to that used in the image representation task, with the only difference being that the polynomial degree is set to 256.

Results: As shown in Fig. 8, our method’s results achieve the best quantitative and qualitative performance, demonstrating our approach’s effectiveness. Specifically, $\text{SL}^2\text{A-INR}$ achieves the highest PSNR at 27.52 dB, indicating superior reconstruction quality. INCODE follows with 26.05 dB, while SIREN, WIRE, ReLU+P.E., and Gauss show progressively lower PSNR values. The visual results demonstrate the effectiveness of our method in capturing the vehicle’s details, including the bucket, tracks, and overall structure.

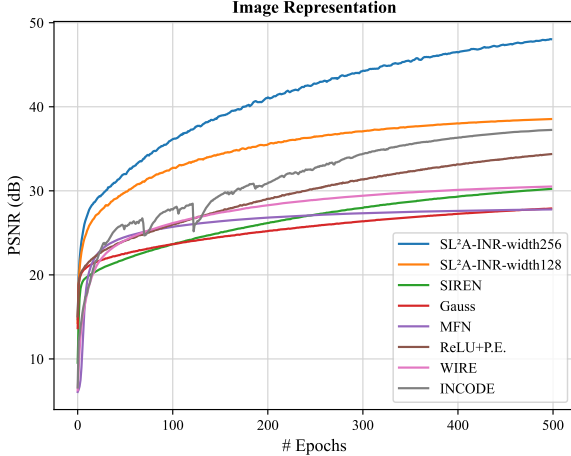


Figure 11: Convergence rate of different models in image representation.

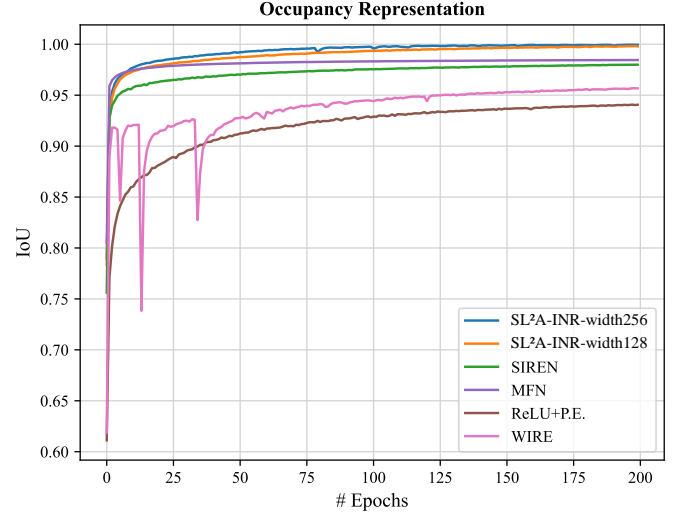


Figure 12: Convergence rate of different models in occupancy representation.

C Further Analysis

Effect of Model Size

Fig. 9 and Fig. 10 demonstrate the superior performance of our model compared to existing methods, even with a significantly smaller network size. In both the floral and architectural examples, our model (particularly the reduced SL²A-INR-width128) outperforms more complex architectures like MFN and ReLU+P.E., preserving intricate details with remarkable accuracy. These results confirm that the effectiveness of our method is not merely due to model size but retaining high-frequency details with remarkable fidelity is rooted in its innovative design. SL²A-INR consistently delivers high-quality results across various scenarios, proving its versatility and efficiency.

Convergence Rate Comparison

We examine the convergence rate of SL²A-INR relative to other methods in two different representation tasks: image, and occupancy volume, as illustrated in Fig. 11, and Fig. 12. Our method demonstrates rapid and superior convergence compared to other approaches. In Fig. 11, the SL²A-INR variants (both width 256 and 128) show the steepest ascent and highest PSNR values across epochs with a clear gap, indicating faster and better image representation quality. Similarly, we achieved the highest occupancy representation values and reached convergence earlier than other methods in Fig. 12. This suggests that SL²A-INR efficiently captures and represents complex data structures with high fidelity in fewer training iterations.

References

Azad, R.; Asadi-Aghbolaghi, M.; Fathy, M.; and Escalera, S. 2019. Bi-directional ConvLSTM U-Net with densely connected convolutions. In *Proceedings of the IEEE/CVF international conference on computer vision workshops*, 0–0.

Bian, W.; Wang, Z.; Li, K.; Bian, J.-W.; and Prisacariu, V. A. 2023. Nope-nerf: Optimising neural radiance field with no pose prior. In *Proceedings of the IEEE/CVF Conference on Computer Vision and Pattern Recognition*, 4160–4169.

Bingham, G.; and Miikkulainen, R. 2022. Discovering parametric activation functions. *Neural Networks*, 148: 48–65.

Cai, Z.; Zhu, H.; Shen, Q.; Wang, X.; and Cao, X. 2024. Batch Normalization Alleviates the Spectral Bias in Coordinate Networks. In *Proceedings of the IEEE/CVF Conference on Computer Vision and Pattern Recognition*, 25160–25171.

Chen, Y.; Wu, Q.; Harandi, M.; and Cai, J. 2024. How Far Can We Compress Instant-NGP-Based NeRF? In *Proceedings of the IEEE/CVF Conference on Computer Vision and Pattern Recognition*, 20321–20330.

Chen, Z.; Chen, Y.; Liu, J.; Xu, X.; Goel, V.; Wang, Z.; Shi, H.; and Wang, X. 2022. Videoinr: Learning video implicit neural representation for continuous space-time super-resolution. In *Proceedings of the IEEE/CVF Conference on Computer Vision and Pattern Recognition*, 2047–2057.

Fakhry, D.; Fakhry, E.; and Speleers, H. 2022. ExSpliNet: An interpretable and expressive spline-based neural network. *Neural Networks*, 152: 332–346.

Fathony, R.; Sahu, A. K.; Willmott, D.; and Kolter, J. Z. 2020. Multiplicative filter networks. In *International Conference on Learning Representations*.

Gao, K.; Gao, Y.; He, H.; Lu, D.; Xu, L.; and Li, J. 2022. Nerf: Neural radiance field in 3d vision, a comprehensive review. *arXiv preprint arXiv:2210.00379*.

Goyal, M.; Goyal, R.; and Lall, B. 2019. Learning activation functions: A new paradigm for understanding neural networks. *arXiv preprint arXiv:1906.09529*.

Heidari, M.; Azad, R.; Kolahi, S. G.; Arimond, R.; Niggebeier, L.; Sulaiman, A.; Bozorgpour, A.; Aghdam, E. K.; Kazerouni, A.; Hacihaliloglu, I.; et al. 2024a. Enhancing

Efficiency in Vision Transformer Networks: Design Techniques and Insights. *arXiv preprint arXiv:2403.19882*.

Heidari, M.; Kolahi, S. G.; Karimijafarbigloo, S.; Azad, B.; Bozorgpour, A.; Hatami, S.; Azad, R.; Diba, A.; Bagci, U.; Merhof, D.; et al. 2024b. Computation-Efficient Era: A Comprehensive Survey of State Space Models in Medical Image Analysis. *arXiv preprint arXiv:2406.03430*.

Hore, A.; and Ziou, D. 2010. Image quality metrics: PSNR vs. SSIM. In *2010 20th international conference on pattern recognition*, 2366–2369. IEEE.

Kazerouni, A.; Azad, R.; Hosseini, A.; Merhof, D.; and Bagci, U. 2024. INCODE: Implicit Neural Conditioning with Prior Knowledge Embeddings. In *Proceedings of the IEEE/CVF Winter Conference on Applications of Computer Vision*, 1298–1307.

Kolmogorov, A. N. 1961. On the representation of continuous functions of several variables by superpositions of continuous functions of a smaller number of variables. *Doklady Akademii Nauk SSSR*, 108: 179–182.

Liu, Z.; Wang, Y.; Vaidya, S.; Ruehle, F.; Halversen, J.; Soljačić, M.; Hou, T. Y.; and Tegmark, M. 2024a. Kan: Kolmogorov-arnold networks. *arXiv preprint arXiv:2404.19756*.

Liu, Z.; Zhu, H.; Zhang, Q.; Fu, J.; Deng, W.; Ma, Z.; Guo, Y.; and Cao, X. 2024b. FINER: Flexible spectral-bias tuning in Implicit NEural Representation by Variable-periodic Activation Functions. In *Proceedings of the IEEE/CVF Conference on Computer Vision and Pattern Recognition*, 2713–2722.

Maiya, S. R.; Girish, S.; Ehrlich, M.; Wang, H.; Lee, K. S.; Poirson, P.; Wu, P.; Wang, C.; and Shrivastava, A. 2023. Nirvana: Neural implicit representations of videos with adaptive networks and autoregressive patch-wise modeling. In *Proceedings of the IEEE/CVF Conference on Computer Vision and Pattern Recognition*, 14378–14387.

Mehmeti-Göpel, C. H. A.; Hartmann, D.; and Wand, M. 2020. Ringing relus: Harmonic distortion analysis of nonlinear feedforward networks. In *International Conference on Learning Representations*.

Mildenhall, B.; Srinivasan, P. P.; Tancik, M.; Barron, J. T.; Ramamoorthi, R.; and Ng, R. 2021. Nerf: Representing scenes as neural radiance fields for view synthesis. *Communications of the ACM*, 65(1): 99–106.

Müller, T.; Evans, A.; Schied, C.; and Keller, A. 2022. Instant neural graphics primitives with a multiresolution hash encoding. *ACM transactions on graphics (TOG)*, 41(4): 1–15.

Ortiz, J.; Clegg, A.; Dong, J.; Sucar, E.; Novotny, D.; Zollhoefer, M.; and Mukadam, M. 2022. isdf: Real-time neural signed distance fields for robot perception. *arXiv preprint arXiv:2204.02296*.

Park, J. J.; Florence, P.; Straub, J.; Newcombe, R.; and Lovegrove, S. 2019. DeepSDF: Learning continuous signed distance functions for shape representation. In *Proceedings of the IEEE/CVF conference on computer vision and pattern recognition*, 165–174.

Rahaman, N.; Baratin, A.; Arpit, D.; Draxler, F.; Lin, M.; Hamprecht, F.; Bengio, Y.; and Courville, A. 2019. On the spectral bias of neural networks. In *International conference on machine learning*, 5301–5310. PMLR.

Ramachandran, P.; Zoph, B.; and Le, Q. V. 2017. Searching for activation functions. *arXiv preprint arXiv:1710.05941*.

Ramasinghe, S.; and Lucey, S. 2022. Beyond periodicity: Towards a unifying framework for activations in coordinate-mlps. In *European Conference on Computer Vision*, 142–158. Springer.

Saragadam, V.; LeJeune, D.; Tan, J.; Balakrishnan, G.; Veeraraghavan, A.; and Baraniuk, R. G. 2023. Wire: Wavelet implicit neural representations. In *Proceedings of the IEEE/CVF Conference on Computer Vision and Pattern Recognition*, 18507–18516.

Shi, K.; Zhou, X.; and Gu, S. 2024. Improved Implicit Neural Representation with Fourier Reparameterized Training. In *Proceedings of the IEEE/CVF Conference on Computer Vision and Pattern Recognition*, 25985–25994.

Sitzmann, V.; Martel, J.; Bergman, A.; Lindell, D.; and Wetzstein, G. 2020. Implicit neural representations with periodic activation functions. *Advances in neural information processing systems*, 33: 7462–7473.

SS, S.; AR, K.; R, G.; and KP, A. 2024. Chebyshev Polynomial-Based Kolmogorov-Arnold Networks: An Efficient Architecture for Nonlinear Function Approximation. *arXiv:2405.07200*.

Su, K.; Chen, M.; and Shlizerman, E. 2022. Inras: Implicit neural representation for audio scenes. *Advances in Neural Information Processing Systems*, 35: 8144–8158.

Sun, Y.; Liu, J.; Xie, M.; Wohlberg, B.; and Kamilov, U. S. 2021. Coil: Coordinate-based internal learning for imaging inverse problems. *arXiv preprint arXiv:2102.05181*.

Tancik, M.; Srinivasan, P.; Mildenhall, B.; Fridovich-Keil, S.; Raghavan, N.; Singhal, U.; Ramamoorthi, R.; Barron, J.; and Ng, R. 2020. Fourier features let networks learn high frequency functions in low dimensional domains. *Advances in neural information processing systems*, 33: 7537–7547.

Timofte, R.; Agustsson, E.; Van Gool, L.; Yang, M.-H.; and Zhang, L. 2017. Ntire 2017 challenge on single image super-resolution: Methods and results. In *Proceedings of the IEEE conference on computer vision and pattern recognition workshops*, 114–125.

Vonderfecht, J.; and Liu, F. 2024. Predicting the Encoding Error of SIRENs. *Transactions on Machine Learning Research*.

Wu, Z.; Jin, Y.; and Yi, K. M. 2023. Neural fourier filter bank. In *Proceedings of the IEEE/CVF Conference on Computer Vision and Pattern Recognition*, 14153–14163.

Xu, D.; Wang, P.; Jiang, Y.; Fan, Z.; and Wang, Z. 2022. Signal processing for implicit neural representations. *Advances in Neural Information Processing Systems*, 35: 13404–13418.

Xu, Z. J. 2018. Understanding training and generalization in deep learning by fourier analysis. *arXiv preprint arXiv:1808.04295*.

Yüce, G.; Ortiz-Jiménez, G.; Besbinar, B.; and Frossard, P. 2022. A structured dictionary perspective on implicit neural representations. In *Proceedings of the IEEE/CVF Conference on Computer Vision and Pattern Recognition*, 19228–19238.

Zeyde, R.; Elad, M.; and Protter, M. 2012. On single image scale-up using sparse-representations. In *Curves and Surfaces: 7th International Conference, Avignon, France, June 24-30, 2010, Revised Selected Papers 7*, 711–730. Springer.

Zhu, H.; Xie, S.; Liu, Z.; Liu, F.; Zhang, Q.; Zhou, Y.; Lin, Y.; Ma, Z.; and Cao, X. 2024. Disorder-invariant implicit neural representation. *IEEE Transactions on Pattern Analysis and Machine Intelligence*.